DESIGN AND INITIAL PERFORMANCE OF A 20 MeV HIGH CURRENT SIDE COUPLED CAVITY ELECTRON ACCELERATOR*

E. A. Knapp and W. J. Shlaer
University of California, Los Alamos Scientific Laboratory
Los Alamos, New Mexico

We would like to describe briefly the Los Alamos Meson Factory project, giving some of the characteristics of the 800 MeV linac at the heart of the facility, particularly by describing the design and performance of the electron prototype accelerator which has been built to investigate many of the features of the LAMPF accelerator.

The gross design characteristics of LAMPF are illustrated in Fig. 1. The pre-accelerator will be a 750 kev Cockroft-Walton high voltage set with a duoplasmatron ion source. The linear accelerator which comprises LAMPF will be made up of two parts, a drift tube accelerator of novel design operating at 201.25 MHz accelerating to 100 MeV, and a side coupled accelerator accelerating from 100 to 800 MeV. We expect an average current of 1000 μA with a duty factor of 6% in the initial phases expandable to 12% as high power electronics become available. With an average rf power of 3 Mw and a beam power of 800 kw, the system is really very efficient in turning electrical energy into beam energy, without suffering an unduly poor duty factor as a consequence of this.

The main purpose of this facility is to make extremely intense pion and muon beams for elementary particle and nuclear structure research. The beams available are really rather impressive and are shown in Fig. 2. The extremely high intensities indicated for these beam intensities will allow wholly new experimental studies to be made using pions as projectiles, using different techniques and perhaps yielding unexpected new results in this energy region which was passed over so rapidly 10 years ago or so. Louis Rosen has published several extensive discussions of the physics possible with this accelerator, and we will not discuss these things here.

The construction schedule for LAMPF calls for beam in the middle of 1972. The present condition of the site is shown in Fig. 3. The injector building will be built in the large flat area in the background, the beam tunnel will be located in the slot, buried under 30 feet of dirt, and the experimental area is located at the near end. The earth in this part of the world is composed of a compacted and cemented volcanic ash rock called tuff, an almost ideal foundation for an accelerator. The square block shown on the experimental area leveled region is 8 tons/sq.ft. of steel directly on this tuff rock. This is the load required for the first indication of failure, however, the foundation has now stabilized and no further motion has been observed. The other really nice feature of this material for a foundation is that while it is rock, it can be worked with a blade and no blasting was necessary for the construction of the channel seen in Fig. 4. For the benefit of amature archeologists, there were approximately a dozen prehistoric indian dwellings in the general area of the site, and these were all excavated before construction work started.

Fig. 5 shows the construction time schedule for the building and site development. The contract for the equipment test laboratory building has been let and construction is underway. The bids for the 100 MeV facility were opened in April and construction will be started in May.

The general outline of the accelerator is shown in Fig. 6.

In LAMPF the acceleration from 100 to 800 MeV will be done in 45 side-coupled accelerator tanks, each driven by a 1.25 MW klystron tube which has automatic phase and amplitude control circuitry to maintain the coherence of the accelerating fields in the accelerator. The Electron Prototype Accelerator (EPA) has been built to investigate the properties of the side-coupled standing wave accelerator tanks in an environment and with constraints on its operation similar to those imposed by LAMPF. The electron prototype accelerator has a buncher-preaccelerator, driven by a 100 kW klystron, and the main accelerator tank driven by the 1.25 MW klystron used for LAMPF. Phase and amplitude control are required, and the performance of the klystron-accelerator tank system for LAMPF is thoroughly wrung out by operation of the EPA.

Perhaps comparison of EPA with several other electron linacs will point up some of the features of the LAMPF linac which might not be obvious at first sight. EPA is truly a completely new type electron linac. A typical traveling wave linac of about 25 MeV energy, such as the linac at Livermore built in 1960 by Varian Associates, has the following characteristics

Maximum av current	0.1 mA (100 μA)
Maximum duty factor	0.0004
Maximum energy	27 MeV unloaded
Peak rf drive power	10 MW.

Another interesting example is the new high intensity electron linac at N.B.S., where

Maximum av current	600 μA
Maximum duty factor	0.002
Maximum energy	170 MeV
Loaded energy	100 MeV
Maximum beam power	60 kW av
rf drive power	60 MW peak, 120 kW av

(12 5 MW klystron tubes)

This represents about the best that normal electron linac technology has done as far as high current, high duty factor operation is concerned. The new MIT linac is designed for higher duty factor operation, but it is not operational yet.

Now contrast that with the LAMPF Electron Prototype Acceleraor, which has been built to investigate some of our new ideas in accelerator technology.

Maximum av current	1 mA ? on up
Duty factor	0.06 → 0.12 later
Maximum energy	30 MeV

*Work performed under the auspices of the U. S. Atomic Energy Commission

50% loaded energy	22 MeV
rf drive power	1 MW peak, 120 KW av (1 tube) 100 kW peak, 12 kW av (1 tube)

In these parameters is a really significant change in performance, the most significant being the change in duty factor by almost two orders of magnitude. In this linac we have a duty factor rivaling that obtainable in some synchrotrons, an extremely important feature as far as typical counting experiments are concerned, and of crucial importance in LAMPF. Also the transfer of rf to peam power is excellent, and manufacture is quite simple.

We shall now briefly discuss how this accelerator differs from the previously built linear accelerators described, then discuss the operating experience obtained so far with EPA, and then we will discuss the experiments planned for EPA and their relationship to LAMPF.

A linear accelerator works by matching the phase velocity of an accelerating wave to the velocity of the accelerating particle, and in fact that principle governs the operation of any rf cyclic accelerator. Just how the interacting wave gets established is radically different in various accelerators, and this is where the new LAMPF EPA design differs significantly from previous linear accelerator systems. The two most used linac cavity designs are the Alvarez standing wave linac tank and the "Hansen" traveling wave iris loaded waveguide. These are shown in Fig. 7.

The drift tube linac uses a standing wave, or resonant, cavity structure, where the electric field is in the same direction in all of the gaps at any one instant of time, and the particle "hides" in the drift tube during field reversal. The distance between gaps is $\beta\lambda$, where λ is the free space rf wavelength and β is the particle velocity. Electromagnetic energy is coupled up and down the cavity by means of the magnetic field outside the drift tube. This is a characteristic "0" mode cavity, the behavior of which we will return to somewhat later. An iris loaded waveguide is also shown in Fig. 7. This is a traveling wave structure, where power is fed into one end of the structure, propagates to the other end and what is left is dissipated in a rf load. To get good utilization of the rf power, an extremely low group velocity must be used in the system, corresponding to weak coupling between cavities in the chain. The phase velocity of the interacting wave is a strong function of frequency and is given by a dispersion relation as shown in Fig. 8. The designer of a conventional electron linac then chooses v_g to give a good attenuation of rf power in the chosen guide length, and then picks a frequency to give the proper v_p to match the particles being accelerated.

This is the cavity system used in almost all electron linacs up until EPA was built, and is the system used in the two examples cited at the beginning of this paper.

For application to a high energy proton linac one would like a resonant system to allow somewhat better control over phase and amplitude of the accelerating wave. Also one wants high efficiency. For example, consider the iris loaded waveguide operated as a resonant system (see Fig. 9), which is the same as before, except terminated in reflecting planes. Then the same dispersion relation as was shown before may be drawn, but in this case instead of a continuous response with frequency we have a number of discrete resonances as shown in Fig. 9 where the π mode is shown above, the zero mode is the one with all fields in line, and the $\pi/2$ mode is field, 0, reversed field, 0, field.

The mojor innovations in the design of linacs in the last few years are (1) to realize that the system as shown above need not be periodic and (2) to realize that the $\pi/2$ mode has special properties which make it especially suitable for accelerator application[1,2,3,4].

We will start by discussing the point that the $\pi/2$ standing wave mode is unique and especially suited to linear accelerator use. Tow examples of the $\pi/2$ mode behavior will be used for illustration although there are many more available. Again, going back to the simple sketch of the iris loaded resonant waveguide, the $\pi/2$ mode has a field distribution as shown in Fig. 10. Now suppose the cavity walls are not perfect, but are lossy, and suppose a beam is passing through the system, which also acts like an additional loss, or alternatively a weak drive in each on-line cavity. Then power must flow between cavities to keep the field distribution equalized. How does the power propagate between excited cavities in the $\pi/2$ mode? A weak field is developed in the "empty" cavities, in quadrature, in such a way that the overlap integral between the cavities of the E x H (poynting vector) permits power flow across the "empty" cavity. The 90° relationship between the cavity fields means that the electric field in the excited cavity is properly phased with the magnetic field in the "empty" cavity for maximum energy transmission with a minimum field in the "empty" cavity. Power transmission requires no phase shift between "full" cavity fields. In contrast, consider the π mode. To get a non-zero value of the overlap integral requires a phase shift between adjacent cavities different than π. This phase shift is loss, and thus beam, dependent.

This property, and many others of a chain of coupled resonators may be studied by means of a "coupled resonator model" for accelerator tanks developed at Los Alamos[3,5].

This model goes like this: we assume a chain of coupled harmonic oscillators with nearest neighbor coupling

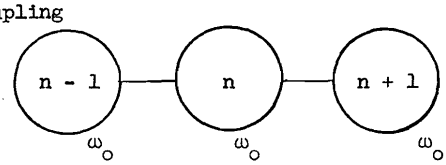

and write down the n + 1 coupled equations of the form

$$I_n = X_n\left(1 + \frac{\omega_o}{j\omega Q} - \frac{\omega_o^2}{\omega^2}\right) + \frac{k}{2}\left(X_{n-1} + X_{n+1}\right)$$

where the I's are drive terms, the Q is the quality factor of the resonator, and where X_n's are amplitudes such that $\sum X_n^2$ = stored energy in cell n.

One immediately gets a dispersion relation for the lossless case

$$\omega_q^2 = \frac{\omega_o^2}{1+k\cos\frac{\pi q}{N}}$$

and eigenvalues

$$X_n^{(q)} \propto \cos\frac{\pi qn}{N} e^{j\omega t} .$$

One interesting result may be obtained by considering the effects of errors in the individual cavity ω's, that is what effect do errors have in the performance of the cavity chains. We have done a perturbation analysis on the above equations and obtain a result

$$\delta X^{\frac{\pi}{2}} = \frac{1}{k}\sum_{\rho=1}^{N} \tilde{\epsilon}_\rho \frac{\sin\frac{\pi\rho n}{N}\sin\frac{\pi}{2}n}{\sin\frac{\pi\rho}{N}}$$

where the $\tilde{\epsilon}_\rho$ is the Fourier transform of the frequency error $\epsilon_n = (\delta\omega_{on}/\omega)^2$. This result has a very interesting property. Recall that in π/2 mode even cavities were excited, odd cavities were not excited. Now, sin π/2 n for n even is zero -- thus, δX(n) = 0 for all even n. So to first order cavity fields do not depend on cavity frequency errors at all! Estimates of the magnitude of second order effects indicate that

$$\frac{\delta X^{\frac{\pi}{2}}}{X} \simeq \left(\frac{\overline{4\Delta\omega}}{k\omega}\right)^2 N$$

@ 805 MHz, k = 0.05, N = 100 $\frac{\Delta\omega}{\omega} = 10^{-4}$ for 1% error (80 kc). This is a fantastically loose tolerance compared to typical requirements on accelerator tanks operating in other modes. The coupled resonator model also gives accurate predictions for many of the other properties of standing wave modes in long chains of cavities, and these have been detailed previously.

So we have shown that the π/2 mode has unique properties all by itself for accelerator service. Next, we ask, what can we **really** do to make the accelerator system as flexible as possible to take advantage of the properties of this mode. At this point we realized that the system does not need to be periodic to support the π/2 mode, and several modifications come to mind. Figure 11 shows the π/2 mode for three different configurations; one periodic, the others not. The first modification into a bi-periodic system consists of maintaining the resonant conditions but making the cavities alternately longer and shorter, thus increasing the efficiency of the system by allowing more of the accelerator's total length to be filled with electric field. Moving the empty cavities off the beam line allows another bit in shunt impedance to be gained, and removes the coupling function from the beam aperature, which then allows the resultant cavity shape to be altered at will to increase the efficiency even further.

Intuitively you would expect that adding capicative loading to the cavity near the beam line would concentrate the electric field near the axis, thus increasing the efficiency. Also this increases the transit time factor by putting the electric field in the center of the cell where interaction will take place with the particle at peak field and over a time interval which is only a fraction of a rf cycle. Lastly, curving the outer wall of the cavity can reduce losses for it minimizes surface to volume ratio (Fig. 12).

We have developed a program which enables one to calculate the detailed structure of the electromagnetic fields in a cylindrically symmetric cavity of arbitrary cross section, and we have used this program to develop a family of cavities shaped as above which have optimized shunt impedance. The final side coupled cavity chain looks as shown in Fig. 13. The final shunt impedance of these cavity chains is more than a factor of two better than the equivalent traveling wave iris loaded waveguide as had been used previously, and a factor of 3 better than possible standing wave iris loaded structures operated in π mode. However, we still can exploit even further the requirement that the π/2 mode system need not be periodic. Figure 14 shows Model M, where adjacent on-line cavities are not the same length, to give a varying phase velocity to the interacting wave.

In LAMPF we require focusing doublets quite often along the length of the accelerator to confine the beam radially. Suppose we would, from power dissipation requirements, like tanks considerably longer than allowed by the spacing between magnets. Then in the side coupled chain we really make it nonperiodic and pull a few excited cavities clear off axis. We then clearly have a single tank electrically but two tanks as far as the beam is concerned. This simple innovation allows a reduction of about a factor of 10 in temperature control tolerances, and removes all high power rf power splitters from the system. The final configuration is shown in Fig. 15. The combination of characteristics above, that is efficiency, and stability make possible the radically different operating characteristics cited earlier. In fact, the possibility of a C. W. Linear Accelerator is certainly not out of the question, and has been seriously proposed by research workers at Chalk River for the ING project. Enough of the technical changes in the waveguide part of our linac. Why did we build EPA?

The prototype accelerator has been built to check out all of these new innovations in accelerator design, and to do several other things. It will allow us to

1. check out above.
2. test phase and amplitude control in the high power rf system.
3. investigate the problems associated with computer control of the LAMPF accelerator.
4. investigate the problems associated with high power dissipation targets in the exact configuration envisioned for LAMPF.
5. investigate the excitation of transverse deflecting modes in structures of this type.
6. investigate fabrication techniques we will use for the LAMPF accelerator.

The general layout of the system is shown in Fig. 16. We start with a pulsed electron gun at 100 keV, accelerate to 1.3 MeV with Model M (the variable phase velocity linac described briefly) using a 100 kW peak klystron amplifier to provide power, and then accelerate to final energy with four tanks of $\beta = 1.0$ length cavities coupled with bridge cavities. The power for the last four tanks is provided by a 1 MW klystron amplifier[6]. The space between tanks is adjusted to compensate for the slip of the particles relative to the accelerating wave since their velocity is slightly less than c. Between tanks are located position monitors, current monitors, steering magnets, foucing magnets, etc. The gradient is the same as we will use in LAMPF, which is quite low by comparison to most electron linacs. In the target area we will do target destruction studies, and use the beam for other experimental purposes.

The next series of figures will illustrate the fabrication of EPA. H. G. Worstell is giving a detailed report on the fabrication procedures used in EPA, so my comments will be brief[8]. Figure 17 shows a raw forging and a machined segment before coupling slots were cut. Figure 18 shows the coupling cell parts before assembly. Tuning of the segments and coupling cells was accomplished by removing a small amount of material from the "nose cones" or capacitive loading in the cavities. Figure 19 shows our experimental set-up for performing this operation. The resonant frequency of two segments clamped together without coupling cavity is the same as the $\pi/2$ mode frequency to within 50 kHz, and this fact is used in the tuning procedure. Figure 20 shows a cut-away assembly from the EPA. Figure 21 shows the brazing furnace used in the fabrication of EPA, along with a stack of eight segments loaded ready for brazing. Figure 22 shows the vacuum manifold being attached to an accelerator section. Figure 23 shows a bridge coupler section, with waveguide coupling iris. Figure 24 shows a section if EPA during final installation, and Fig. 25 shows the completed accelerator. Figure 26 is a view of the 1.25 MW klystron used to power the accelerator. Figure 27 shows the target area in the EPA.

In every respect so far the operation of EPA has been successful. In late December we turned on the system for the first time and achieved a good beam of ~25 MeV at low current. Subsequently we have achieved all of the operating characteristics outlined above, that is a 1000 μA beam at ~20 MeV, ~1% energy spread, and extremely smooth and reliable operation. How have some of the questions we were wishing to study for LAMPF been answered? Well, first off, the structure works like expected, or even better. Initial tuning indicated the four tanks were flat to ~6%, the variation coming in tank 2 where a gross mistuning (several megacycles) which was uncorrectable caused a field perturbation. The bridge couplers perform as expected, however during initial tune up it became clear that the post couplers in the bridge cavity are essential to eliminate the power flow phase shift across the bridge. We have experienced no trouble with these post couplers, adding to our confidence in the post coupling scheme for the drift tube accelerator. The phase shift measured from end to end of the 100 cell chain was less than 1°, the resolution of our measuring equipment. The mode spectrum about the $\pi/2$ mode is symmetric, as expected, with a 230 kHz mode separation on either side of the operating point. The waveguide coupling hole was enlarged to provide a 1.3/1 VSWR, overcoupled. The measured shunt impedance is ~42 MΩ/m, also very close to the predicted value.

Turn on and tank conditioning was uneventful. The rf power level was raised slowly keeping the outgass pressure below 10^{-5} mmHg and full accelerating gradient and duty factor were achieved in a few hours. Temperature control of the tanks is provided with a closed loop control system which regulates the water temperature to keep the tanks on a fixed resonant frequency, in this case 805.000 MHz. This closed loop system senses the power level in the tank and the tank copper temperature, and adjusts the water temperature to compensate for thermal gradients across various parts of the structure. An 8°F drop in water temperature is required to maintain the water passages and the tank walls. The controller works extremely well and adequately adjusts for this large swing in temperature.

The phase and amplitude closed-loop control systems have worked exceptionally well. Figure 28 shows the field in the tank during a 50 μsec beam pulse of 20 ma amplitude. Even though this beam requires ~30% additional power the amplitude in the tank is nicely controlled by the servo system. In the case of the phase system, Fig. 28 also shows the response. In this case a signal from the tank is compared to a reference phase source, and the input signal to the klystron is phase shifted to produce the proper phase in the cavity. We feel this rather sophisticated control problem, which was a considerable worry at the beginning of our project, has been adequately solved.

No sign of beam blowup or the excitation of transverse modes has been detected, even though we have looked carefully with spectrum analyzers at the fields excited in the tanks. Calculations by R. Gluckstern would indicate we should expect transverse beam blowup well below the currents where we have operated[9]. We attribute this effect to the extreme tolerance of the $\pi/2$ mode to mistunings of the individual cavities, and the destroying of a "flat" transverse mode due to this tolerance of the fundamental mode. Figure 29 shows current transformer signals at six positions down the length of the accelerator. The pulse length is ~500 μsec and the amplitude at the output of the accelerator is 18 ma.

As far as computer control is concerned, we have run the accelerator manually through the computer, and while the computer is not particularly transparent in manual dealings with the accelerator we have managed to bring up a beam and successfully thread it through the accelerator all from on the other side of the computer.

New programs are being written and brought on the air as quickly as possible. One example of the power of computer control was recently demonstrated. A program was written to find the beam and maximize transmission through a collimator by steering with a pair of upstream steering magnets. After a few false starts, this program works

extremely well, making decisions which converge to maximum beam transmission. Most of the operating time on the EPA for the last few months has been used investigating the problems of computer control.

Several extensive rf system experiments have been done with computer data aquisition and will be reported later in this conference. The behavior of the resonant tank with and without beam loading is approximately as expected. However, the details of the klystron-tank interaction are not well understood and work is continuing. It is clear that the klystron cannot be considered an isolated power source and that system-wide interactions must be considered for a complete description. Computer data aquisition really simplified these experiments and it would appear that computer control of large accelerator installations is really a significant step forward.

We have not as yet burned up any targets. The beam is dumped in water now, and as soon as a high pressure water system is finished we will start LAMPF target testing. As far as design for LAMPF is concerned, we are about to start on final mechanical design. We are convinced our approach is sound and that we will be able to achieve the characteristics required for LAMPF.

References

1. E. A. Knapp,"800 Mc RF Structures", 1964 Linear Accelerator Conf.,July 20-24,1964, MURA-714, p. 31.
2. E. A. Knapp, "Design, Construction and Testing of RF Structures for a Proton Linear Accelerator," IEEE Transactions on Nuclear Science, Vol. N.S.-12, No. 3, June, 1965, p. 118.
3. D. E. Nagle, E. A. Knapp and B. C. Knapp, "A Coupled Resonator Model For Standing Wave Accelerator Tanks," RSI,38, 11, p. 1583 (1967).
4. T. Nishikawa, S. Giordano and D. Carter, RSI,37, 5, p. 652-661 (1966).
5. E. A. Knapp, B. C. Knapp and J. M. Potter, "Standing Wave High Energy Linear Accelerator Structures," (to be published in June, 1968 RSI).
6. D. C. Hagerman, "800 MHz Power Sources for LAMPF", Proceedings, this Conf.p.76
7. R. A. Jameson, "Automatic Control of RF Power Systems", Proceedings, this Conf.p.149
8. H. G. Worstell, "Mechanical Design of LASL Linac Structures - (LAMPF)", Proceedings, this Conf.p.1
9. R. L. Gluckstern, D. E. Nagle and W. M. Visscher, "A Note on Transverse Beam Instabilities in Multisection Linacs", Proceedings 1966 Linear Accelerator Conf., Oct. 3-7, 1966, LASL.

DISCUSSION

(E. A. Knapp)

KUNTZE, KARLSRUHE: Is the Q value of the bridge cavity comparable with the Q value of the tanks?

KNAPP, LASL: It is probably slightly higher than the tanks. The Q of the cavities along the beam line is roughly 29,000. The Q value of the bridge cavity should be approximately 30,000 to 35,000.

CHRISTOFILOS, LRL: What is the peak and average current of the model electron accelerator?

KNAPP, LASL: It is 17 mA peak current, 1 mA average current. It is a very low peak current and a high duty factor. The duty factor will be similar for the new accelerator.

GREEN, AECL: What is the buncher efficiency and what fraction of the beam from the gun do you get out of the end of the accelerator?

KNAPP, LASL: We accelerate roughly 40% of the cw beam to 1.3 MeV. We lose about 1/3 or more of the beam in the first tank due to the poor radial qualities of the beam out of the buncher.

GLUCKSTERN, U. of MASS. It might be well to point out that the 18 mA electron current you get, without transverse instability, suggests that proton currents in the ampere range may be obtainable without transverse instability. The ratio of the momenta determines this.

I want to ask about your comment, "that one of the tanks had different frequency characteristics from the rest." I think the estimates of current limits depend critically on having the transverse modes come at exactly the same frequency in each tank.

KNAPP, LASL: If I understand your calculations, the current I quoted is for instability in a single tank. The first tank is most susceptible, and that is not the one that has the problem.

Ion Source: Duoplasmatron - 30 keV

Preaccelerator: 750 keV Pierce-type short column

Alvarez Accelerator:

Frequency 2.0125×10^8 Hz

Structure - Alvarez, 4 tanks

Tank 1	- 0.75	-	5.0 MeV
2	- 5.0	-	41.2 MeV
3	- 41.2	-	72.3 MeV
4	- 72.3	-	100.3 MeV

Waveguide Accelerator:

Frequency 8.050×10^8 Hz

Structure - side-coupled shaped cavities $\pi/2$-mode standing wave

Number of tanks - 90

Current: Peak - 17 mA
Average - 1 mA

Duty Factor: 6 - 12 %

Overall Length: 850 m

Peak RF power for cavity excitation	38 MW
" " " " beam excitation	14 MW
Total	52 MW
Average RF power (6%)	3 MW

Figure 1. Design Parameters for the Los Alamos Linac

Pion Energy (MeV)	Pion Production Cross Section* (cm^2/sr-MeV)	λ Pion Decay Distance (ft)	Positive Pion Intensity (per Sec)	Negative Pion Intensity† (per Sec)
100	10×10^{-30}	34.9	2.8×10^8	5.9×10^7
200	25×10^{-30}	55.5	2.8×10^9	5.9×10^8
300	50×10^{-30}	74.6	1.1×10^{10}	2.4×10^9
400	20×10^{-30}	93.4	7.0×10^9	1.6×10^9
500	5×10^{-30}	111.6	2.4×10^9	5.3×10^8

Conditions:

1 mA average proton beam = 6×10^{15} protons/sec at 800 MeV;

18 g/cm^2 Be target;

3×10^{-3} sr pion channel acceptance;

$\Delta p/p = 6.7\%$, total momentum acceptance of the pion channel;

43-ft channel length.

*Values calculated by Los Alamos Monte Carlo Cascade Code.

†Cross section for negative pions taken as 1/4.5 times that for π^+; ratio calculated by Cascade Code.

Figure 2. Pion Beam Intensities from LAMPF

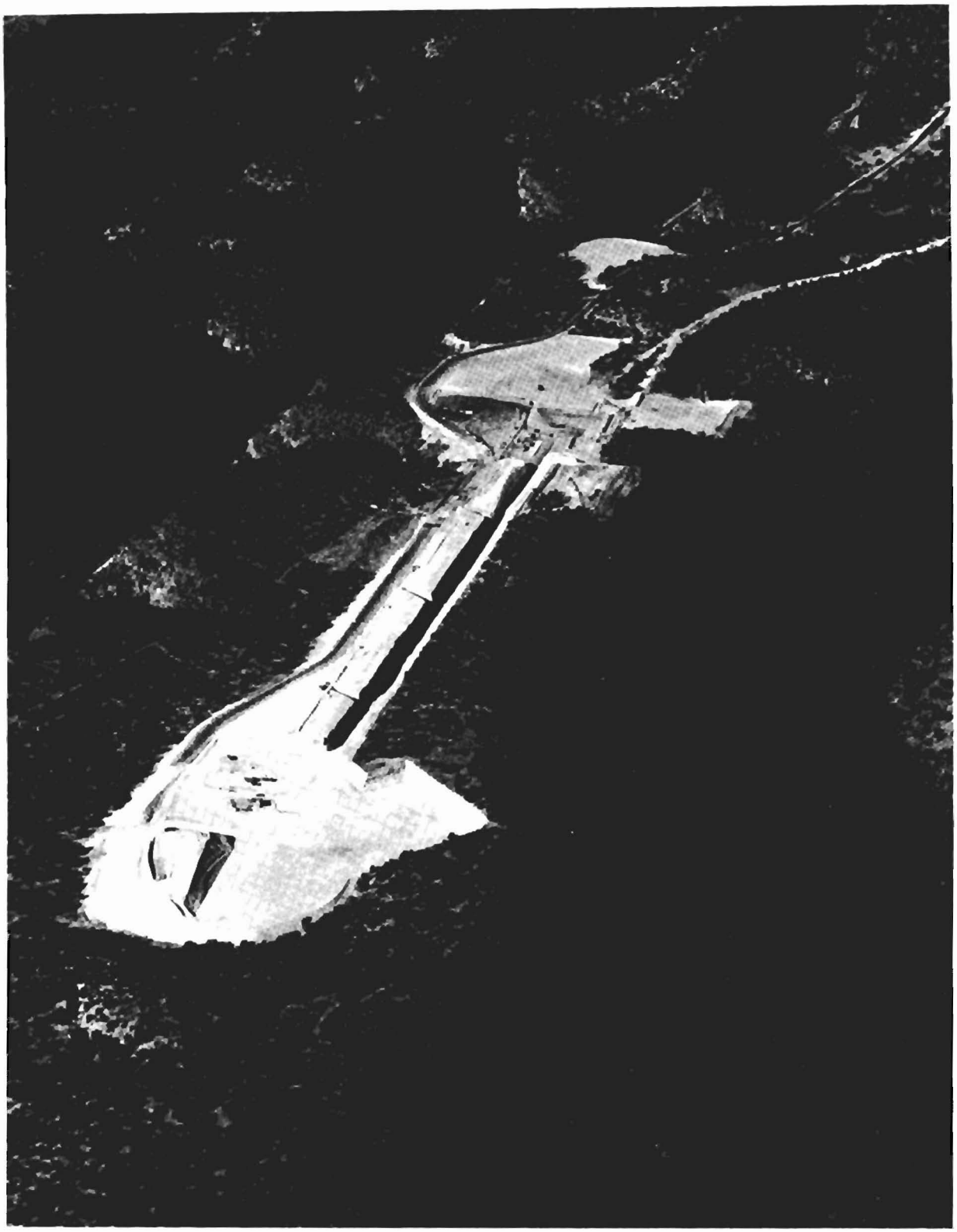

Figure 3. LAMPF Accelerator Site

Figure 4. LAMPF Beam Channel

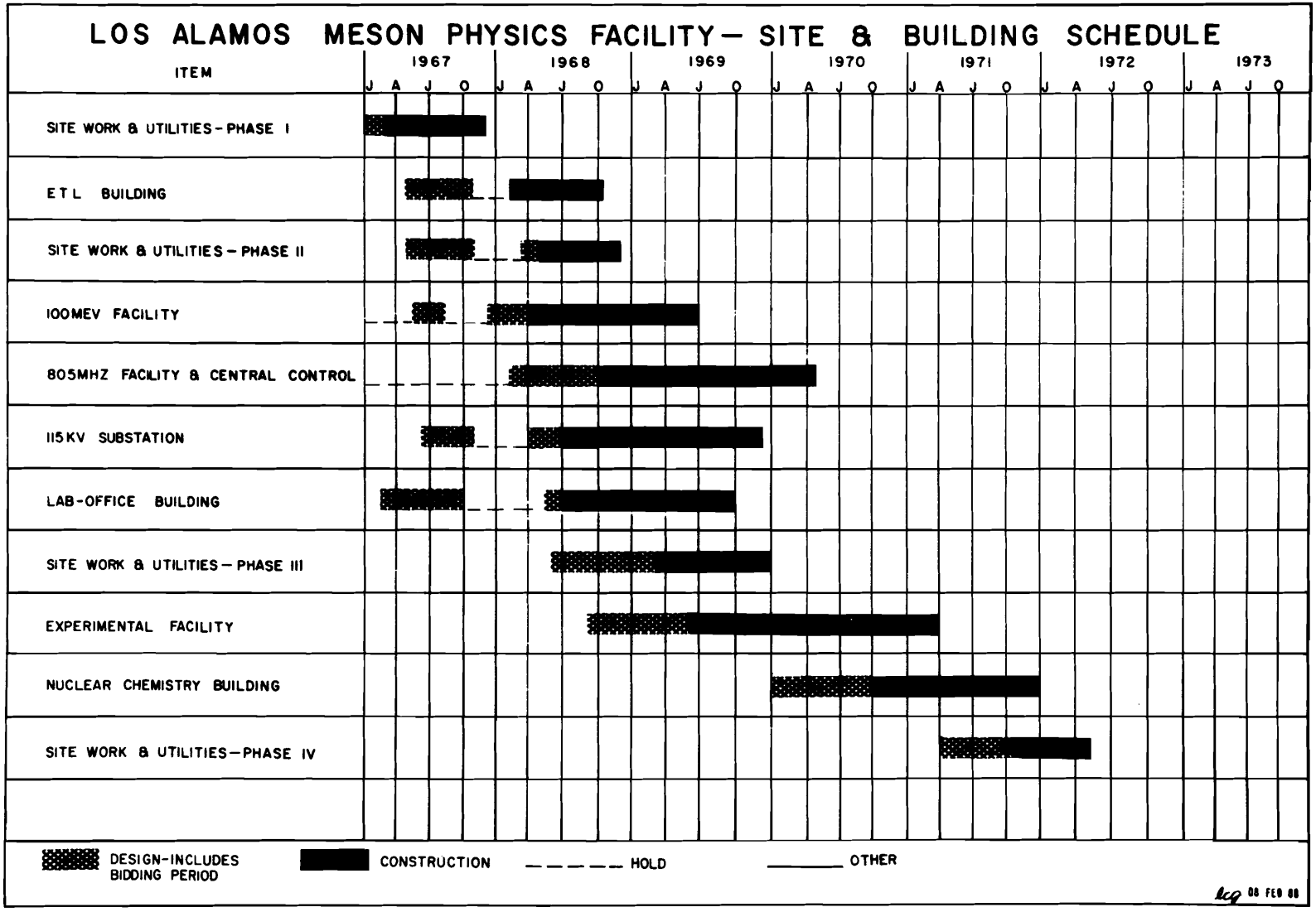

Figure 5. LAMPF Site and Building Schedule

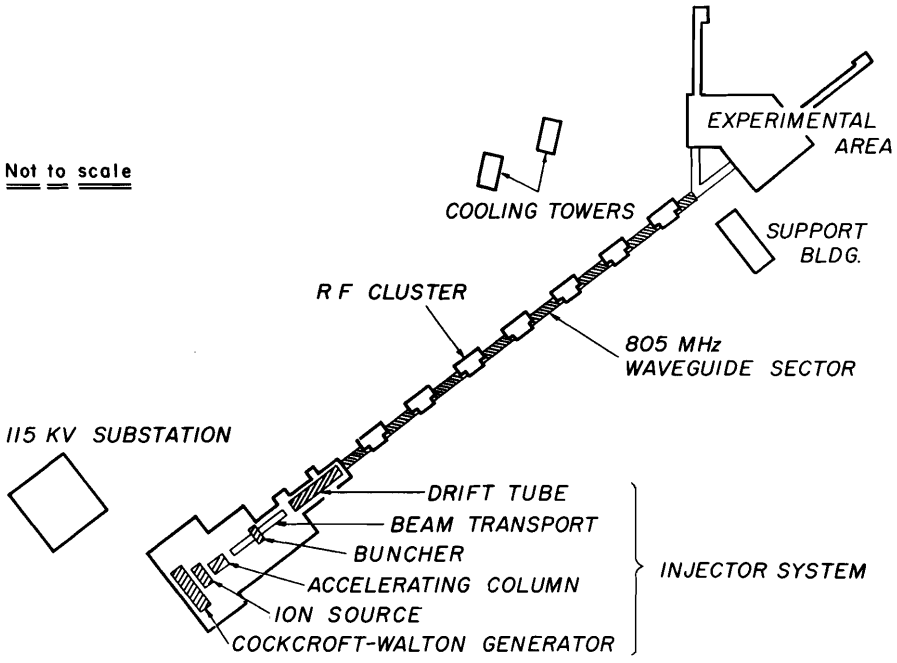

Figure 6. LAMPF Accelerator and Experimental Area

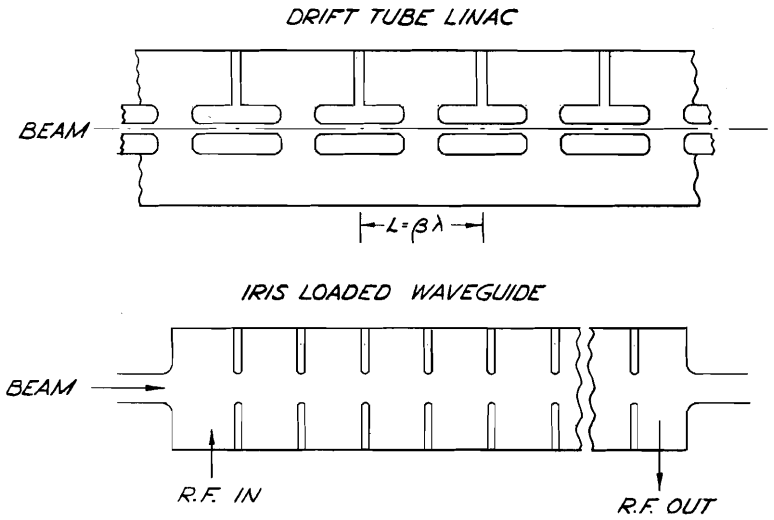

Figure 7. Schematic of Drift Tube Linac and Iris Loaded Waveguide

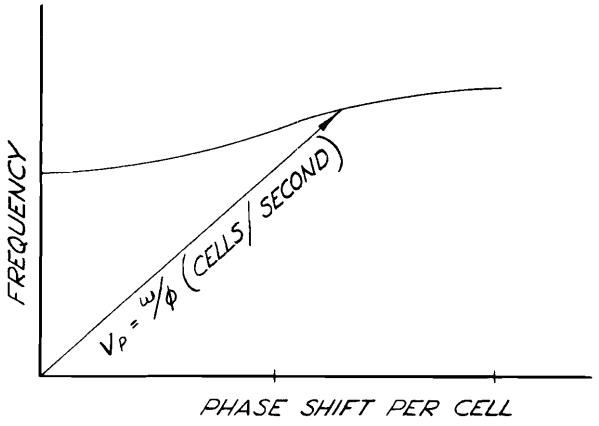

Figure 8. Dispersion Curve for Traveling Wave Linac Guide

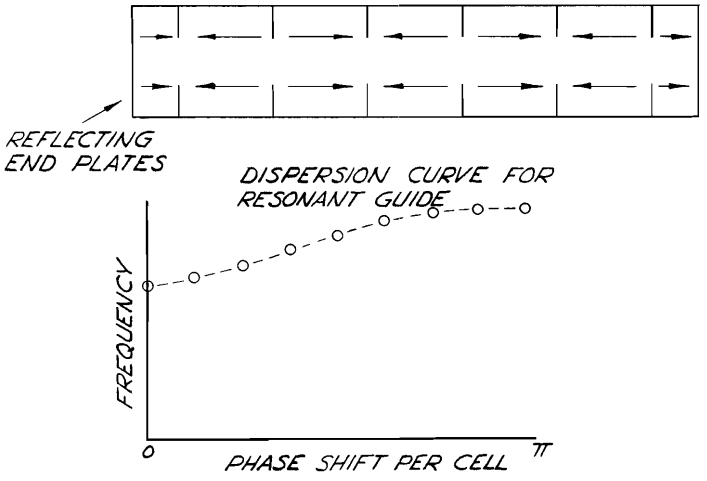

Figure 9. Resonant Operation of Iris Loaded Waveguide

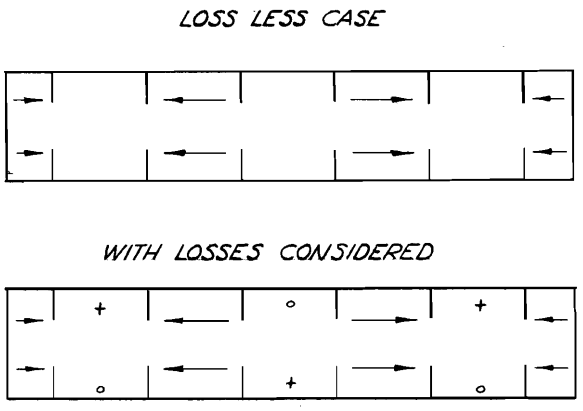

Figure 10. $\pi/2$ Mode Operation of Iris Loaded Waveguide

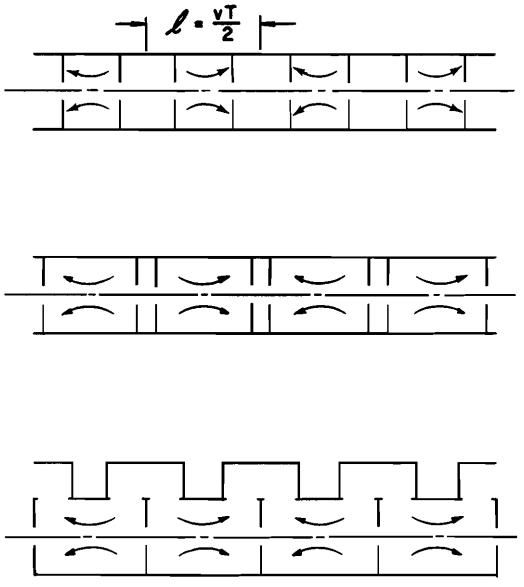

Figure 11. Three Cavity Configurations Operating in $\pi/2$ Mode

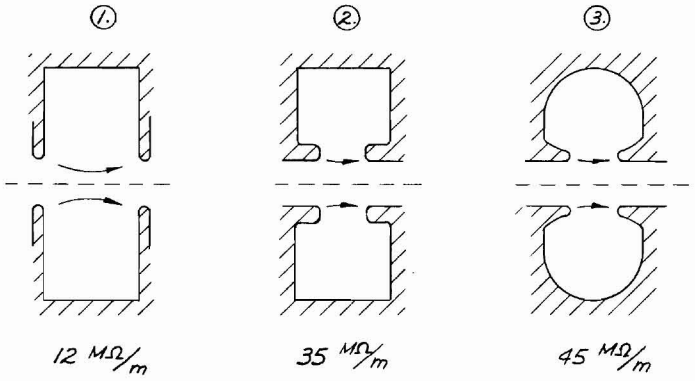

Figure 12. Cavity Geometry Changes to Optimize Shunt Impedance

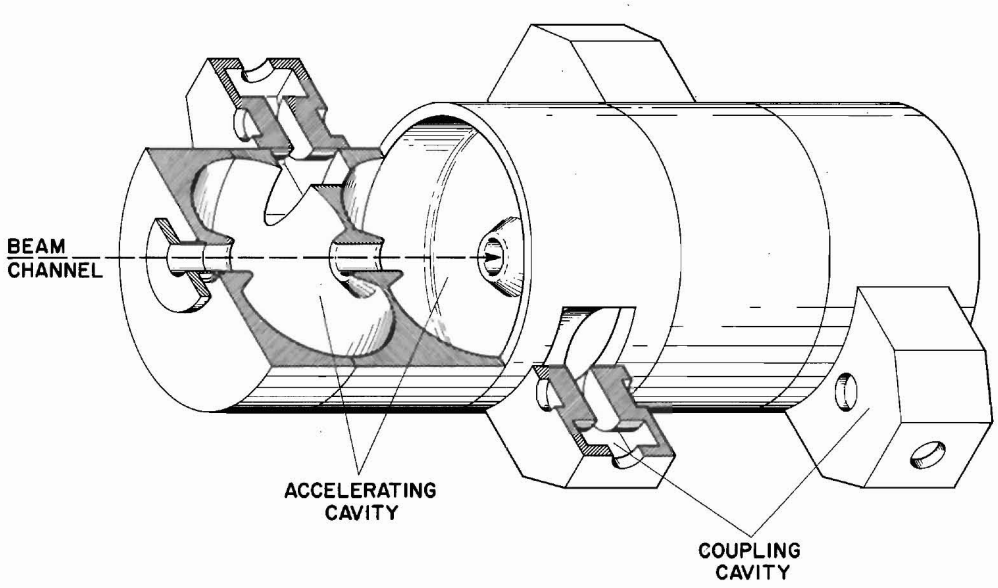

Figure 13. Side Coupled Cavity Configuration for Optimum Shunt Impedance

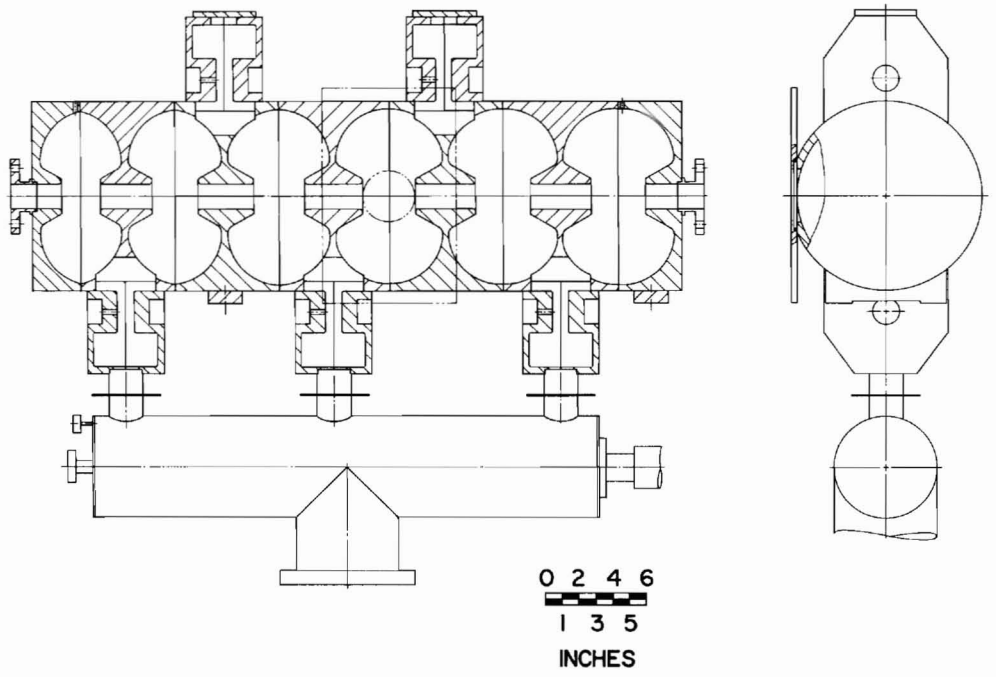

Figure 14. Model M, A Variable Cell Length Side Coupled Cavity Accelerator Tank

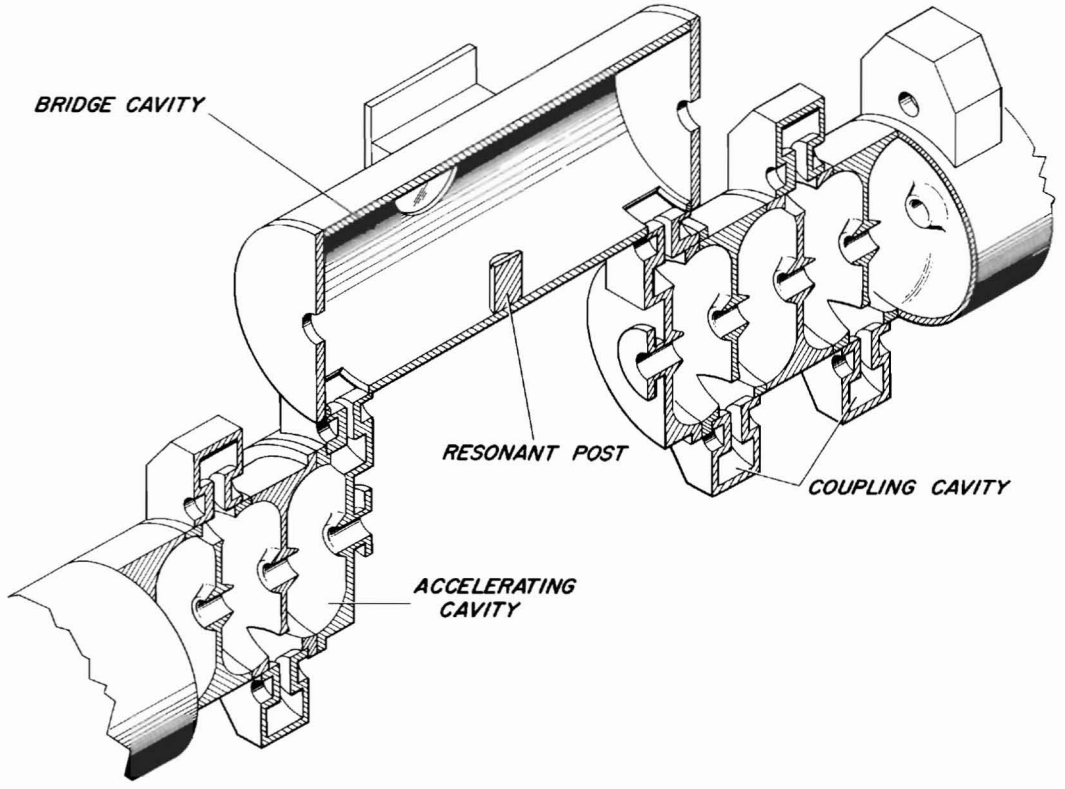

Figure 15. Side Coupled Accelerator Chain With Bridge Coupler

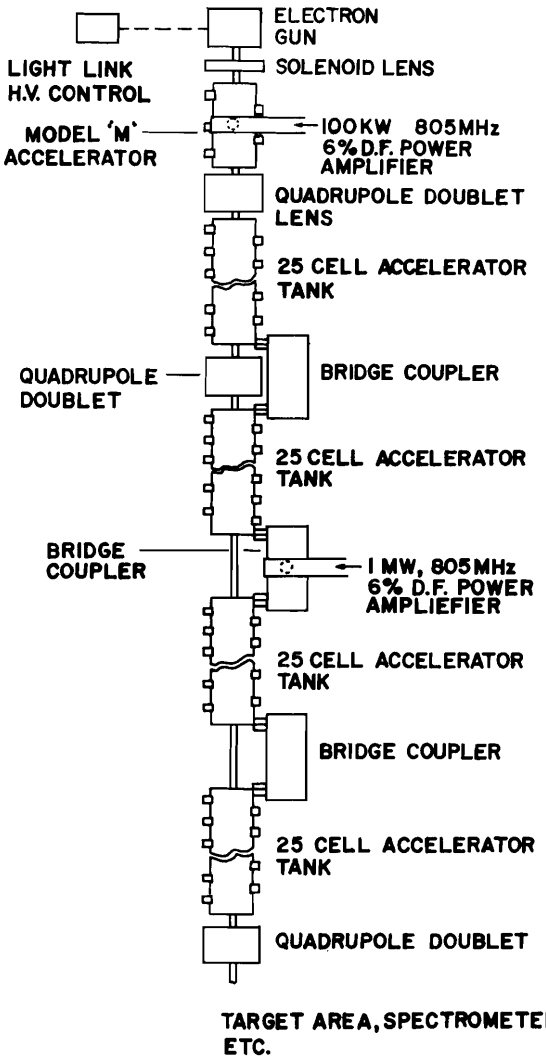

Figure 16. Layout of the Electron Prototype Accelerator

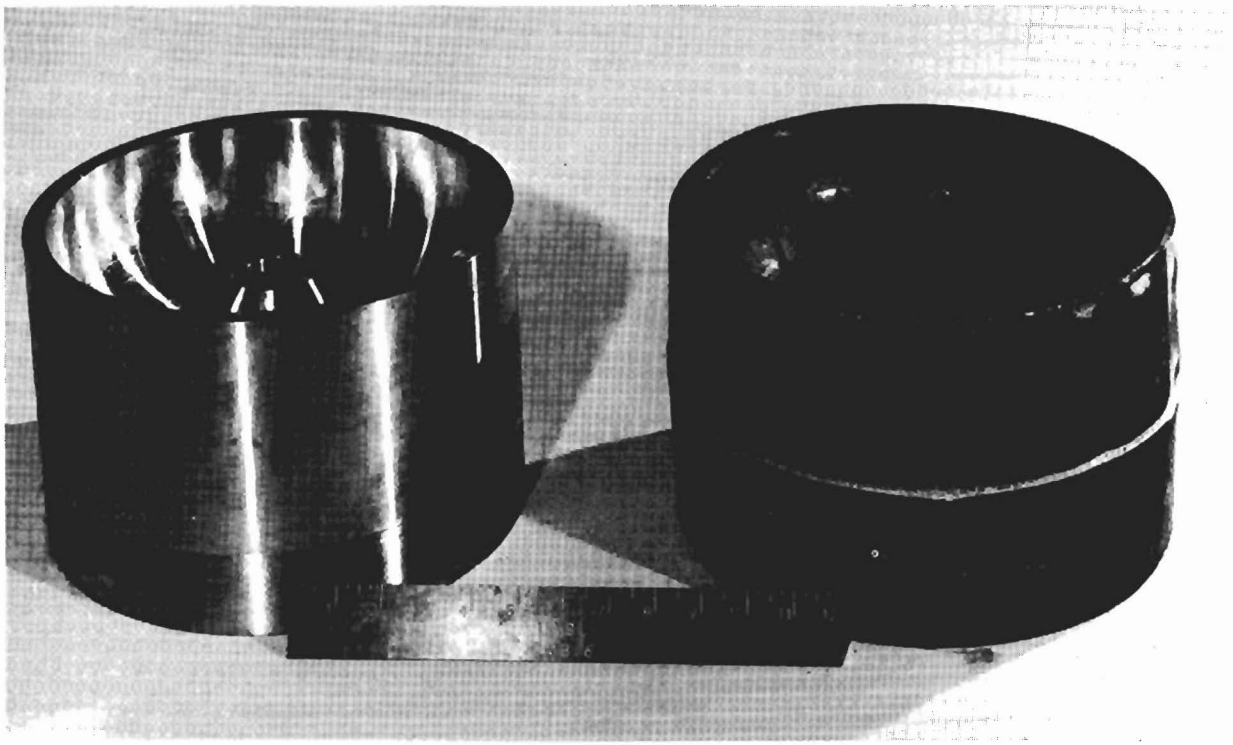

Figure 17. EPA Forging and Machined Segment

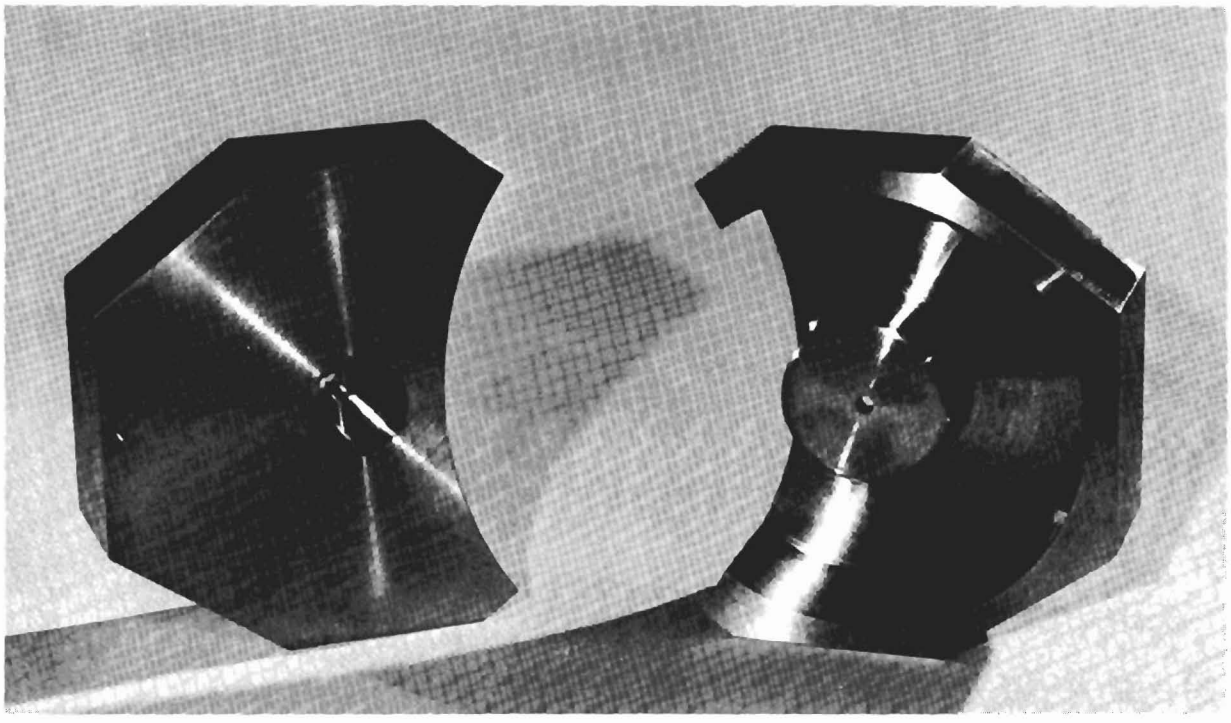

Figure 18. EPA Coupling Cavity Parts

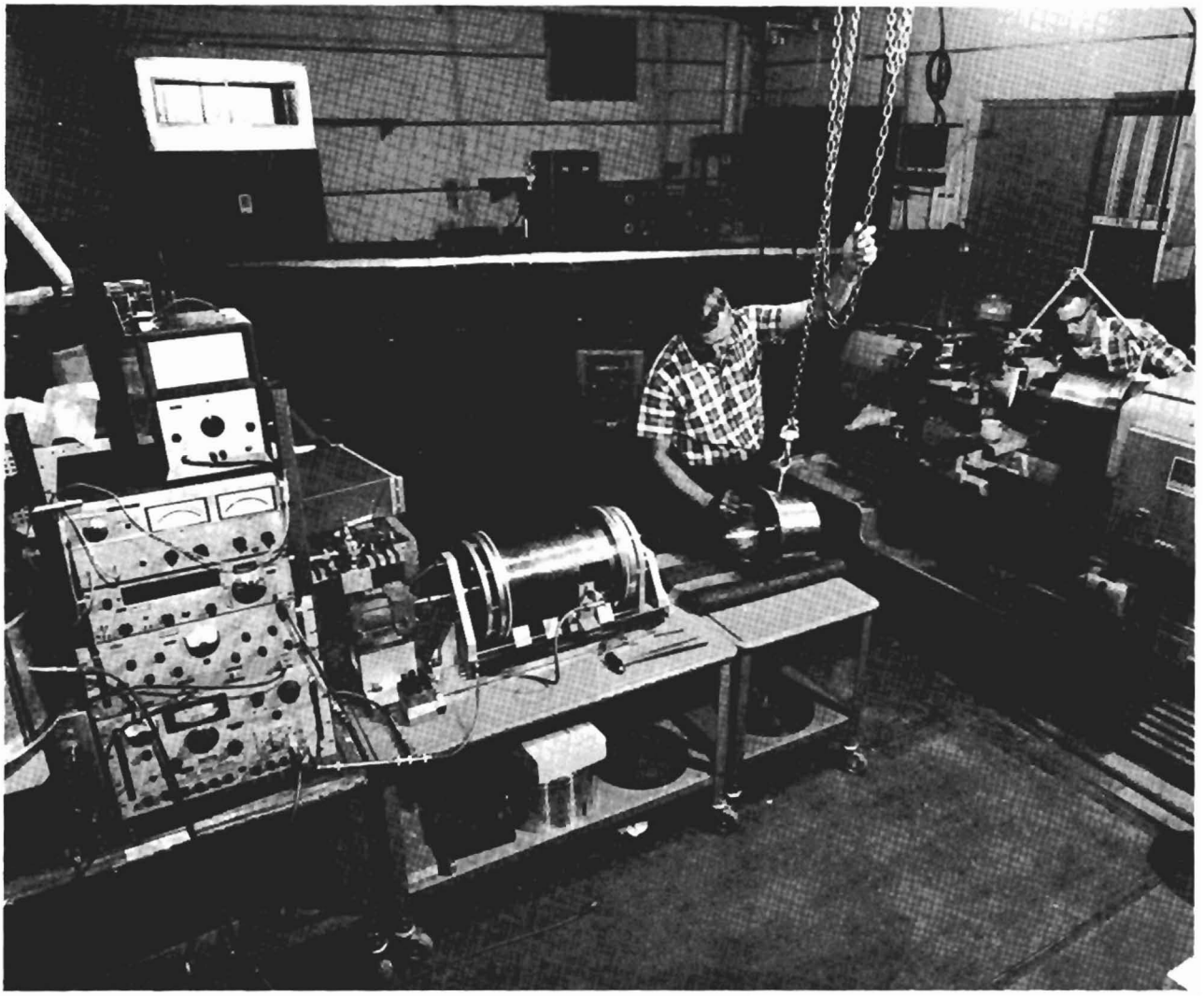

Figure 19. EPA Tuning Lab.

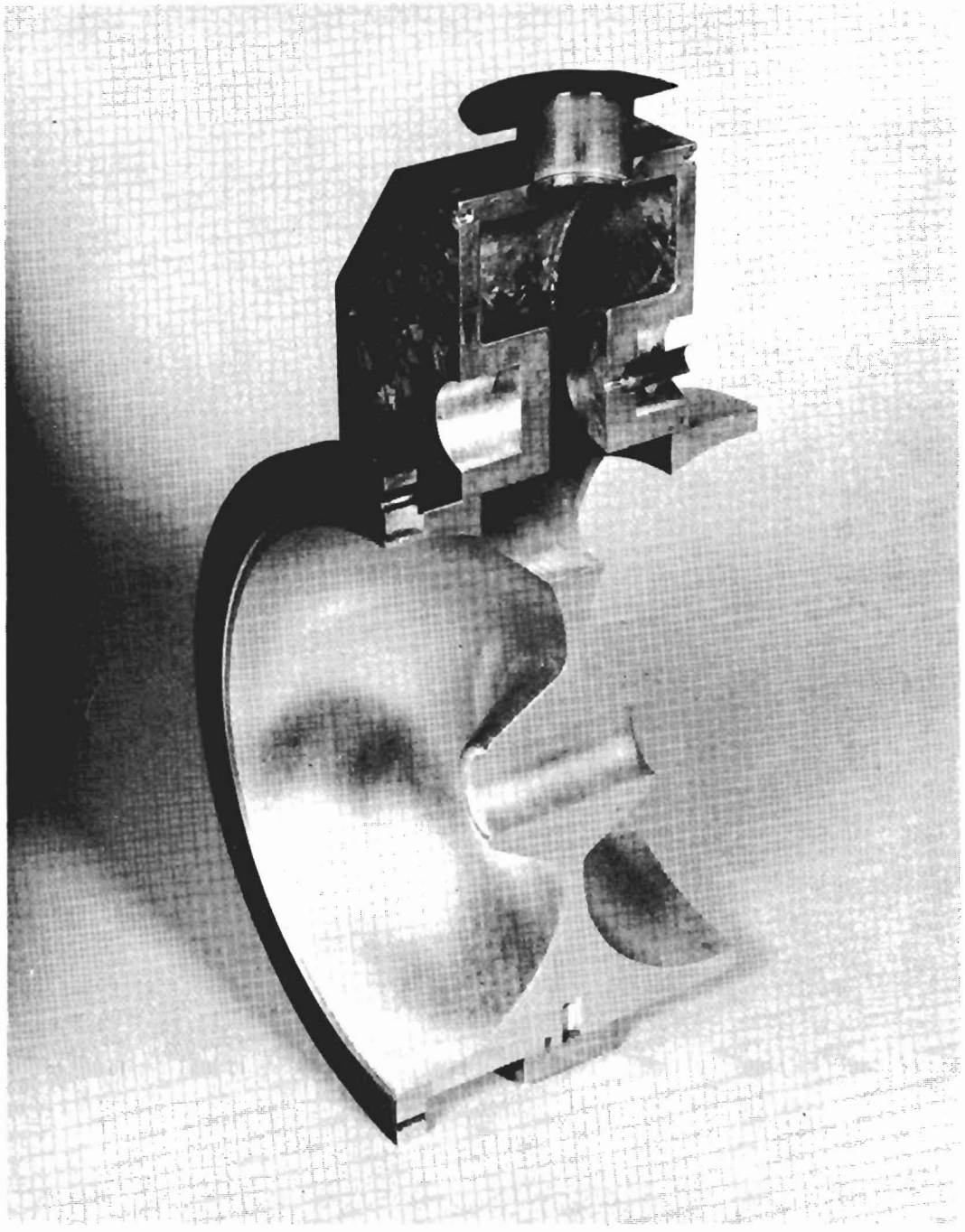

Figure 20. Cut Away Section of EPA Accelerating Segment-Coupling Cell Assembly

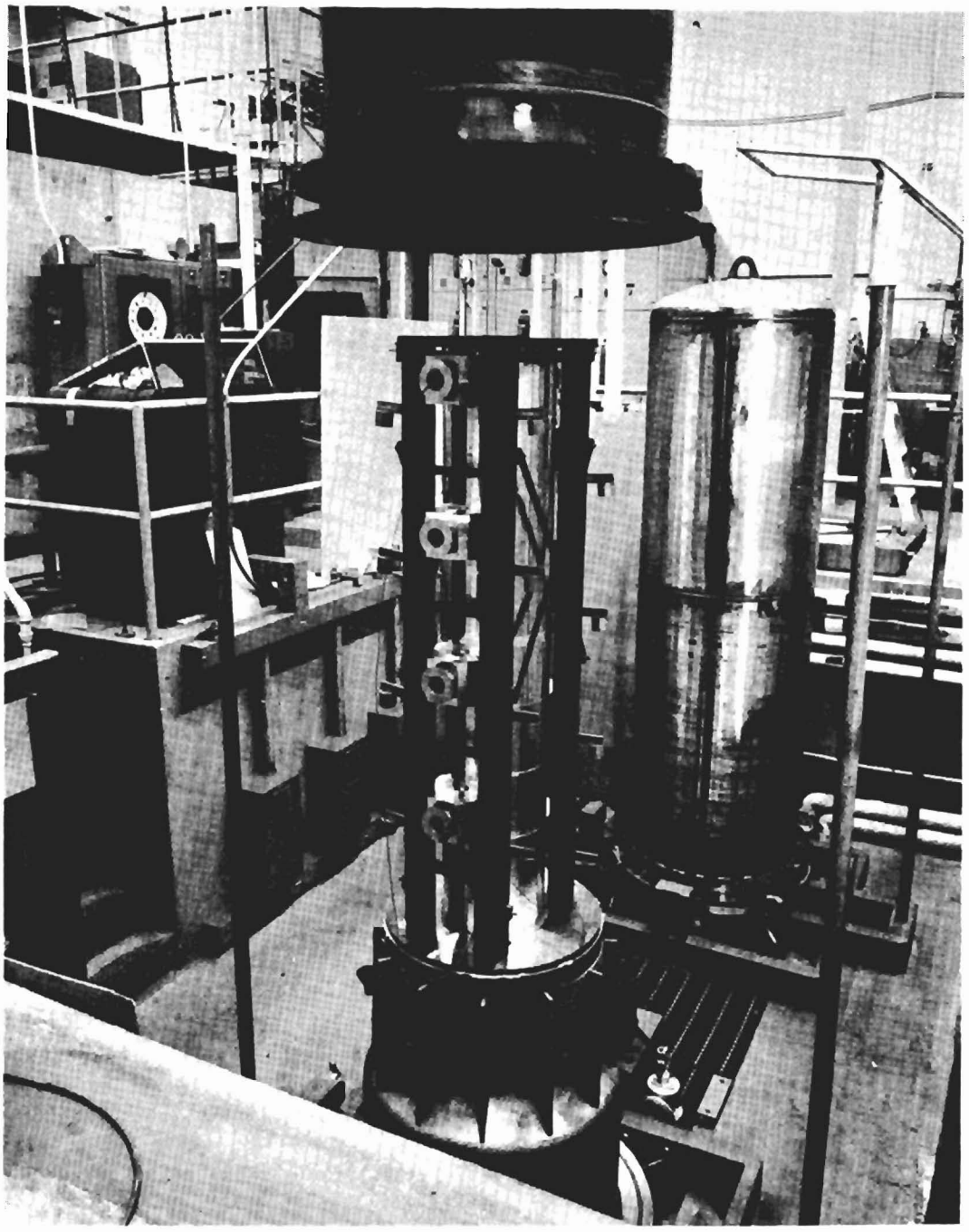

Figure 21. An EPA Tank in Place for Final Braze Operation

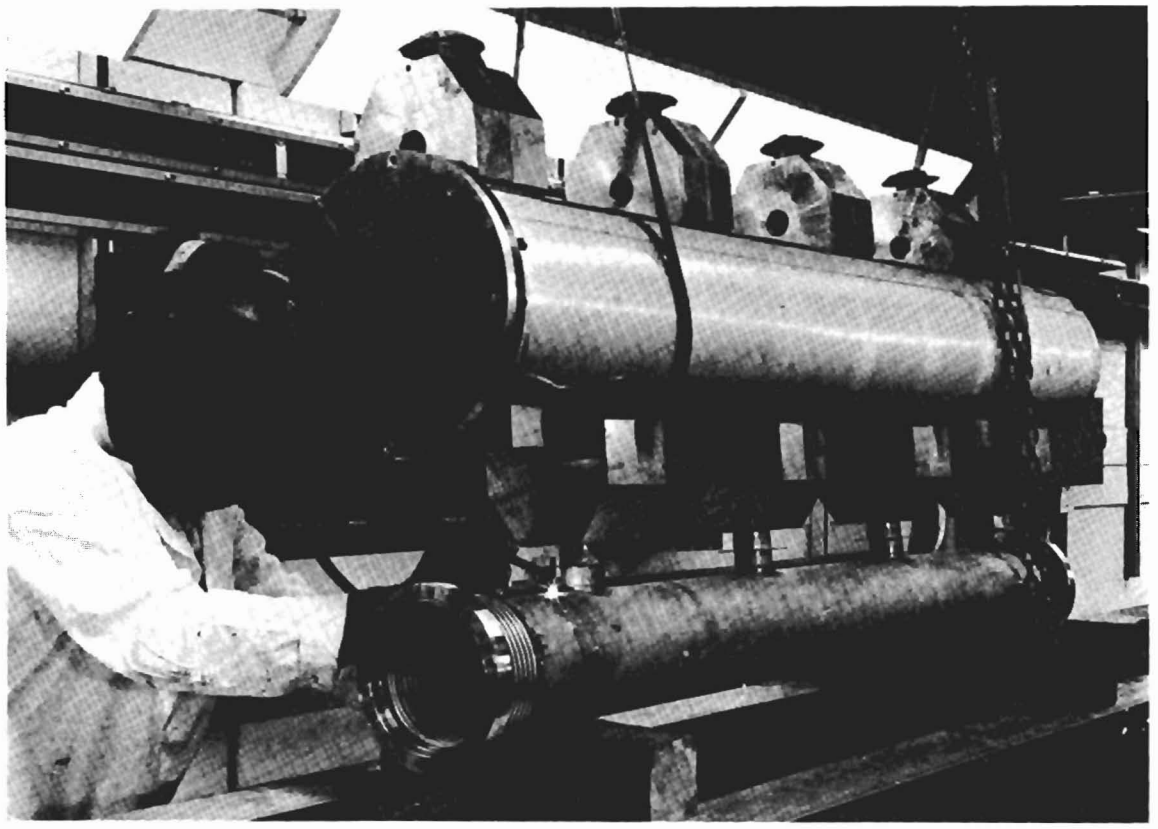

Figure 22. Attachment of Vacuum Manifold to EPA Tank

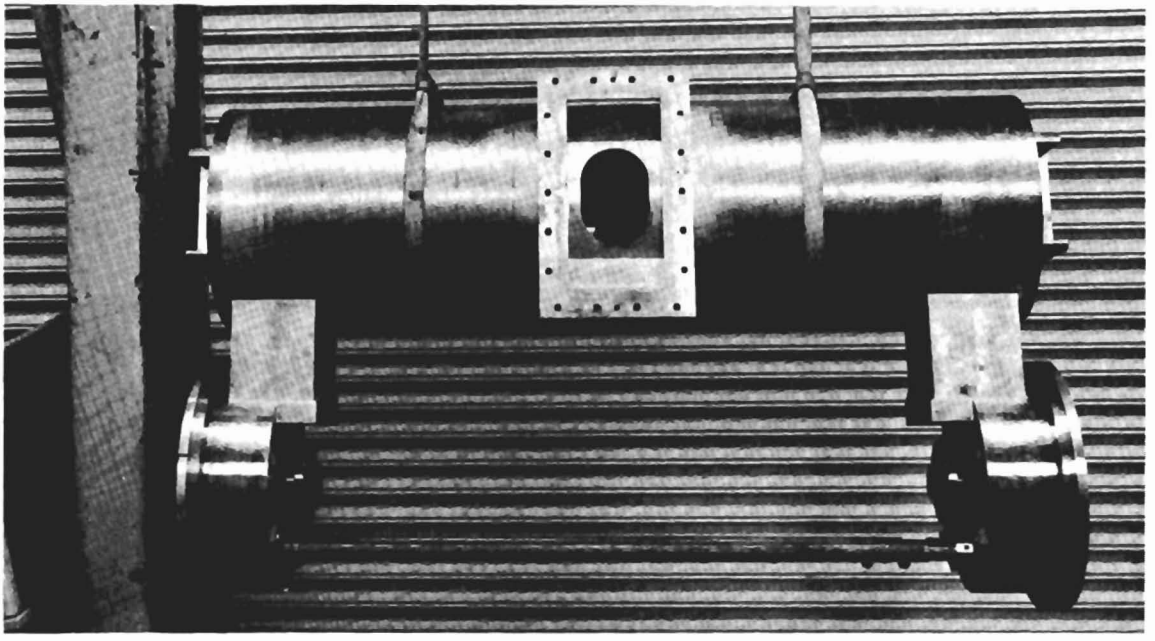

Figure 23. Bridge Cavity for EPA, With Iris Coupling Shown

Figure 24. EPA During Assembly

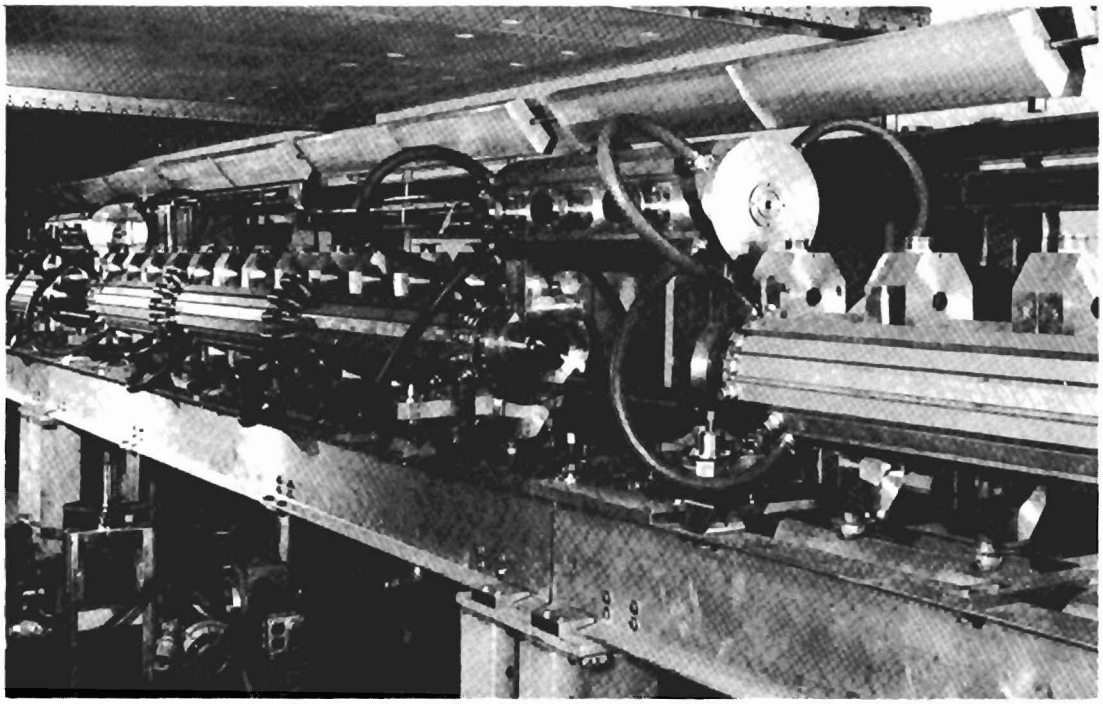

Figure 25. EPA Bridge Coupler During Final Assembly and Tuning

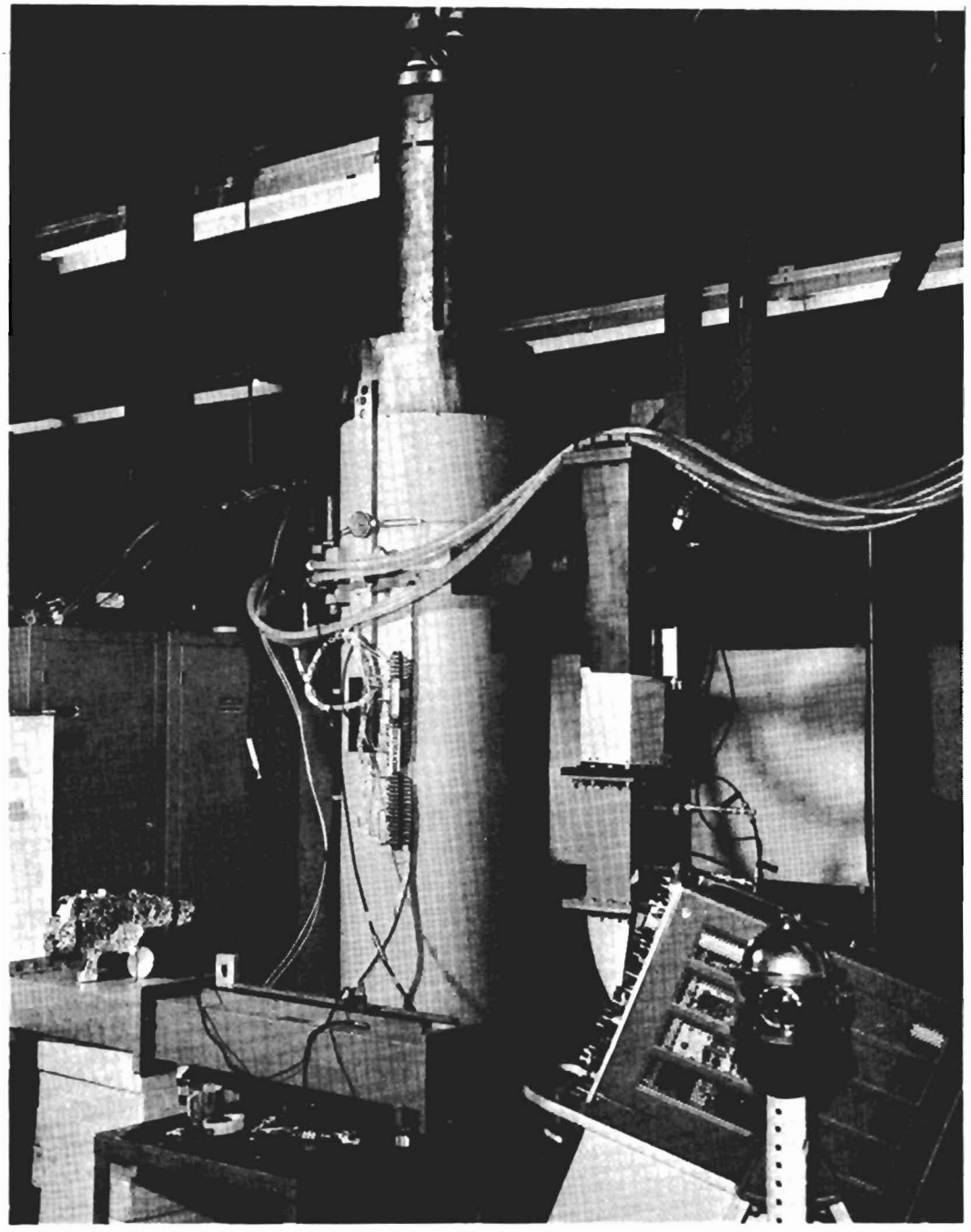

Figure 26. 805 MHz 1.25 MW Klystron Amplifier

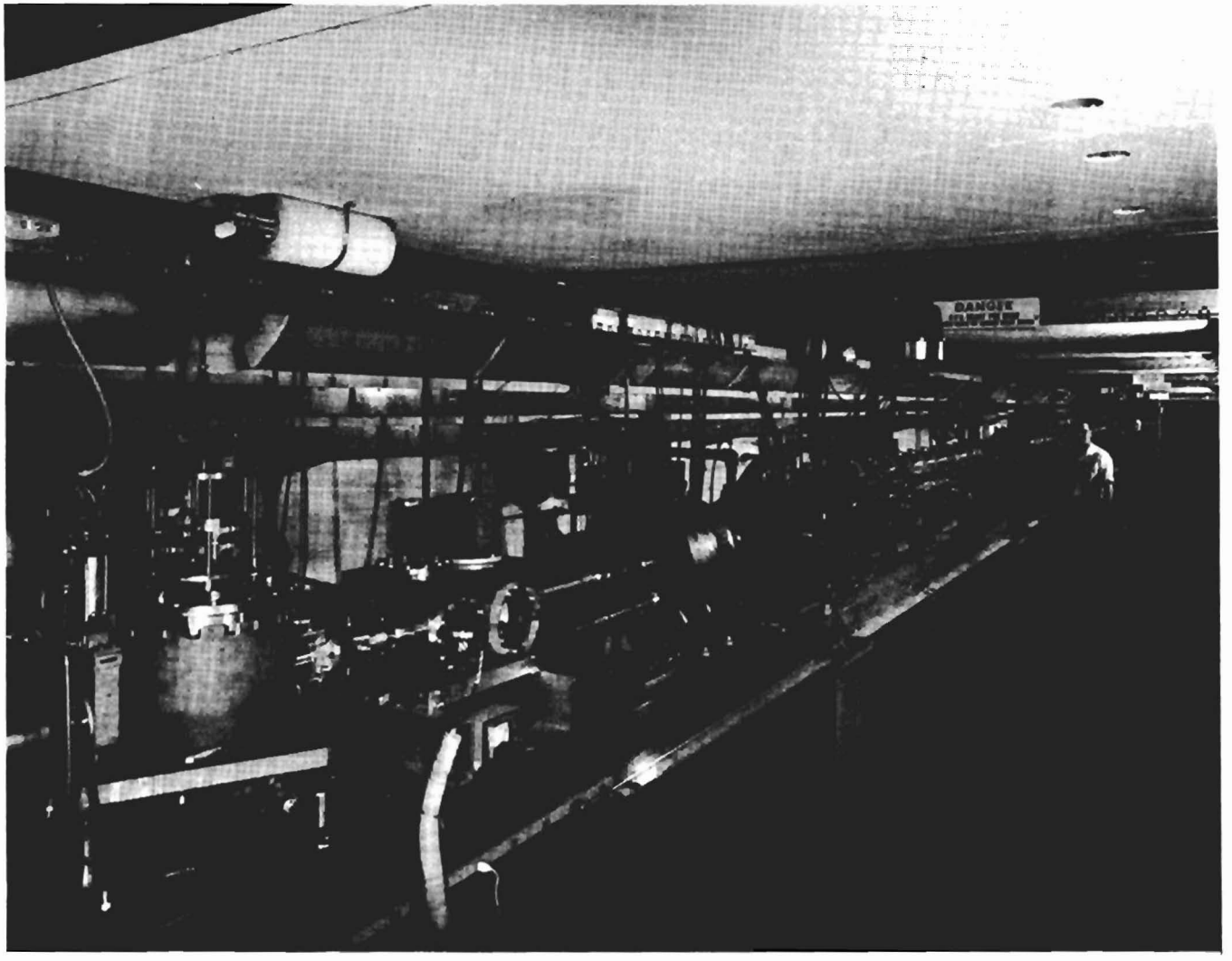

Figure 27. Electron Prototype Accelerator from Target Area

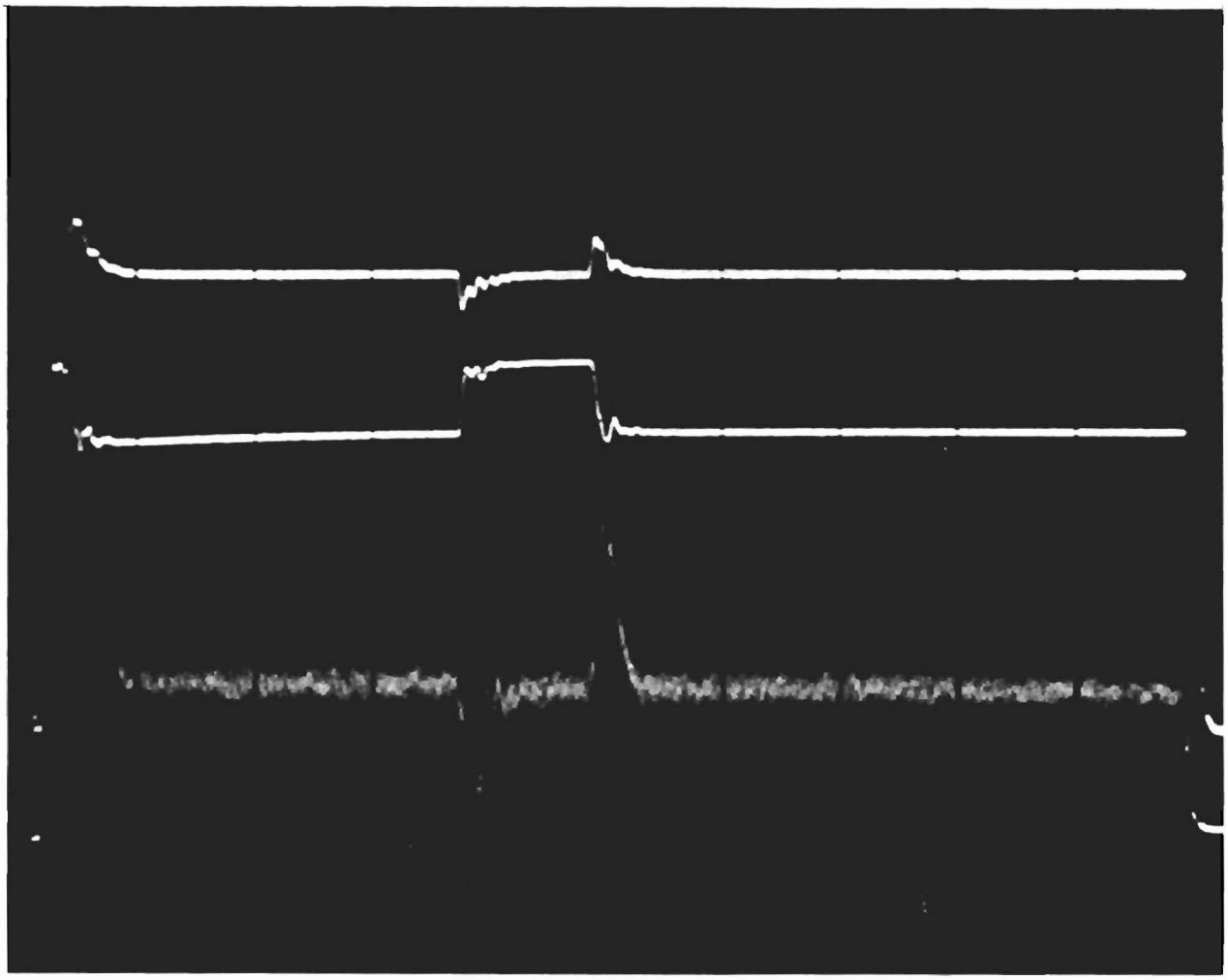

Figure 28. Effect of Beam Loading on EPA RF System. The Top Trace is Field Amplitude in the Tank; Second Trace is Forward Power from the Klystron (Scale not Linear); Third Trace is the Difference in Phase Between the Tank Field and a Reference (~ 2°/cm)

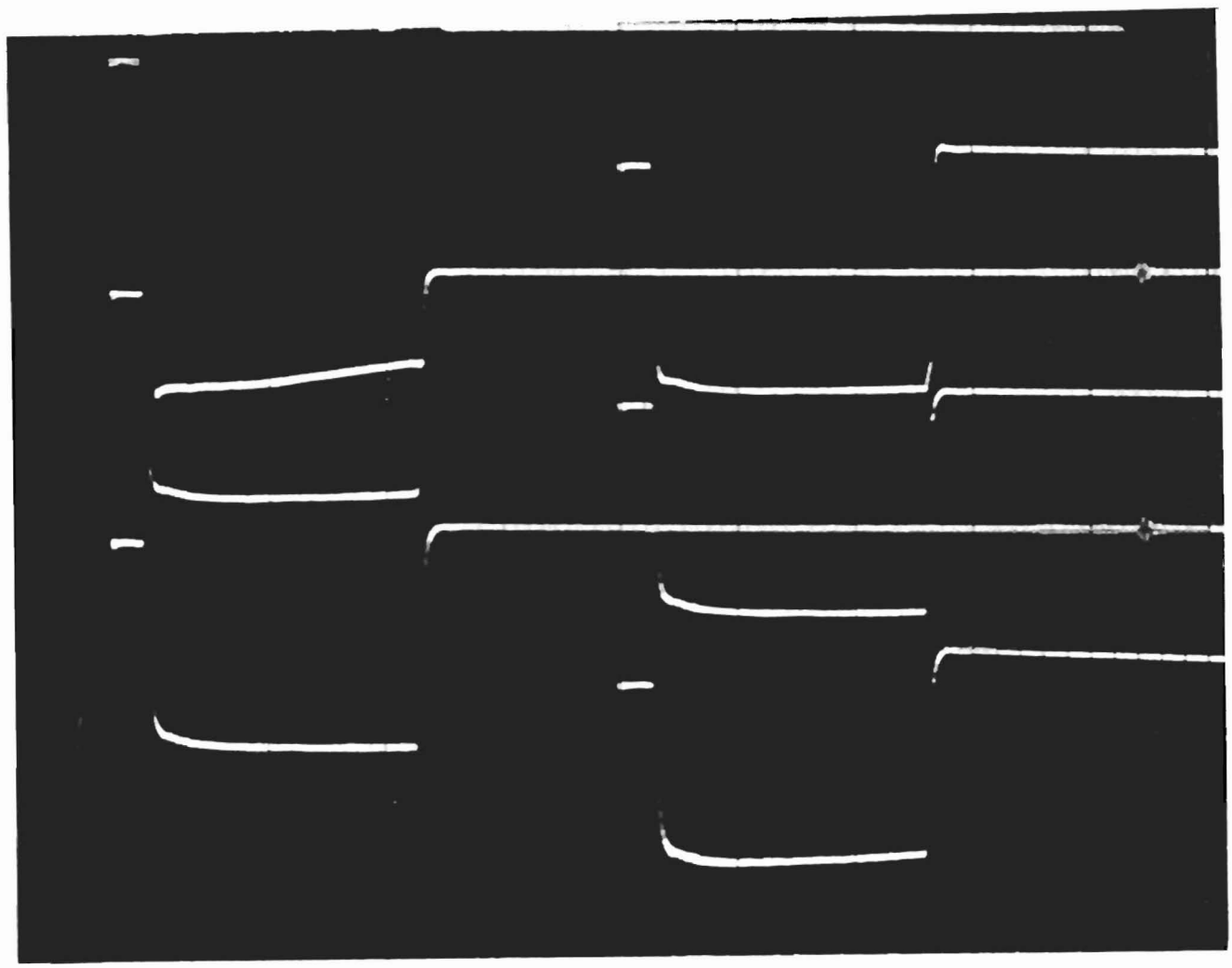

Figure 29. Beam Current Transformer Outputs from EPA Under High Current and Duty Factor Operation. 10 ma/cm Vertical Scale, 200 μsec/cm Horizontal Scale. The Bottom Left Hand Signal is the Output from the Last EPA Tank.